INTERACTION OF PURE TUNGSTEN POWDER WITH PROCESSING CONDITIONS IN SELECTIVE LASER MELTING

A.T. Sidambe, P. Fox

Centre for Materials and Structures
School of Engineering
University of Liverpool
Brownlow Hill
Liverpool, L69 3GH
United Kingdom

Abstract

In this study we consider the role of the pure tungsten powder interaction with processing conditions within Selective Laser Melting (SLM). Tungsten powder (sub 45µm) was subjected to investigations which involved the creation of a process map through single track and single layer hatching studies. The effects of laser power, scanning speed and hatch spacing were studied using the process map parameters. Light optical microscope, scanning electron microscope and X-Ray diffraction techniques were used to analyse the results. The studies showed that for the given laser energy density, the temperature and the volume of the molten powder was higher at lower scanning speeds. The results also showed distinguished grain structures between the x-y horizontal build plane and the z-y vertical build direction. The SLM process was successfully used to fabricate highly dense tungsten of up to 98 % density.

1 INTRODUCTION

Selective Laser Melting is an additive manufacturing (AM) process that is relatively new and is increasingly being used to lower the cost of production, particularly for complex shapes. This has led to SLM being adopted as an alternative to conventional methods such as machining and casting because of its ability to produce near net shape components [1, 2] [3] [4]. SLM can produce functional, custom specific, solid or lattice components in a short space of time without the need for tooling [1]. In the SLM system, a high-powered laser with a power of 200 to 400W is used to fuse metal powder into a solid component based on a 3D CAD file. Components are built one layer at a time using the additive method with the layer thickness typically in the range of 30µm [5-8]. Figure 1 shows a schematic diagram for the SLM process. SLM is also known as direct metal laser sintering (DMLS) or selective laser sintering (SLS).

SLM is currently used commercially for processing of steels, titanium, nickel- and aluminium-alloys in medical and aerospace industries. However, the application of SLM to the processing of high temperature materials such refractory metals has so far been limited because of the intrinsic problems of processing higher melting point materials. The successful development of the processing of refractory metals using SLM is expected to lead to an increase in the application of refractory metals, with these materials used in novel ways. Therefore processing of refractory metals via SLM although technically challenging, would lead to an advantage in the high value manufacturing sectors such as medical implants, rocket nozzles and support hardware [9, 10].

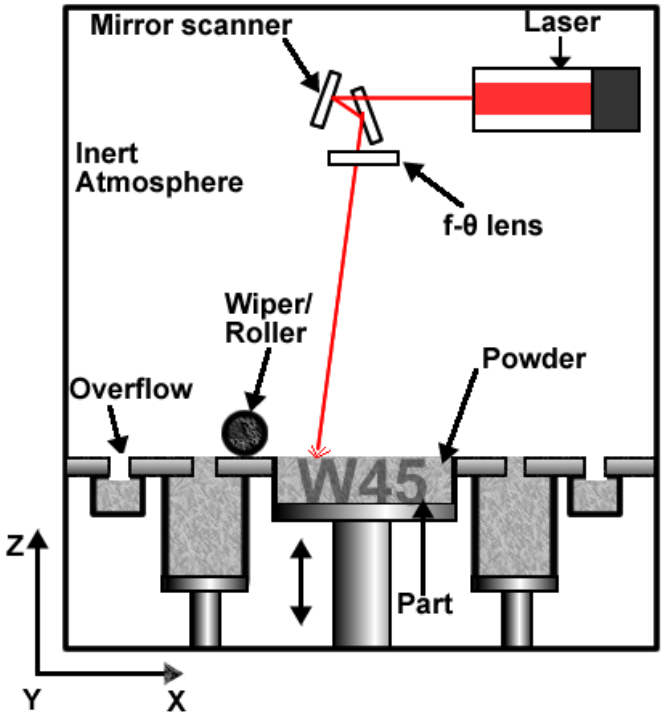

Figure 1: Schematic overview of the selective laser melting (SLM) process

In this study, we identify the barriers that limit the effectiveness of SLM processing of pure tungsten and then evaluate the properties. Tungsten has a very high melting point (3422 °C), high boiling point (5700 ± 200 °C), low vapour pressure and low thermal expansivity. These properties make tungsten an ideal choice of material in ultra-high temperature applications in many technology fields such as military, electro vacuum, crucible and heating elements [11]. In combination with the high density (19.2 g/cm^3), tungsten possesses superior radiation attenuation characteristics, which makes tungsten ideal for use as shielding and in pinhole collimators [12]. However the hardness and strength of tungsten hinders the processing of complicated shaped parts with small dimensions. In these cases, traditional metal working techniques such as milling, casting or pressing cannot be used [11].

Table 1: Physical properties of tungsten

Physical properties	Tungsten
Density at 25 °C (g/cm^3)	19.2
Liquid Density (g/cm^3)	17.6
Melting Point (°C)	3655
Thermal Conductivity (W.m^{-1}.K^{-1})	174
Specific Heat (J.kg.K^{-1})	134
Thermal Diffusivity (m^2/s)	0.068
Atomic mass	183.88
Tension Force (N/m)	2.361

Table 1shows the physical properties of tungsten, some of which make it difficult to process tungsten. Of particular interest are the high melting point, the high thermal conductivity and the high viscosity. In order to overcome the challenges of fabrication with tungsten using conventional methods, there has been a number of studies carried out that investigate the use of additive manufacturing. In one of the early studies, Zhong et al. [13] reported that the use of a tungsten nickel alloy powder was successful when fabricating a collimator using a blown powder process called Laser Engineered Net

Shaping (LENS™), however pure tungsten powder could not be successfully used due to the metal's high melting point [13]. Later on, Ebert et al. used pulsed-laser micro sintering in a study which demonstrated that the density of tungsten parts increased with the applied laser energy [14]. Their results showed that with sufficient power, the processing of pure tungsten should be possible. A year later, Deprez et al. successfully fabricated a complex MR-compatible collimator with a large number of oblique pinholes from pure tungsten powder using selective laser melting [12]. More recently, the intrinsic properties of tungsten and the laser processing parameters were established as being important in the determination of the properties of the SLM produced parts. The study by Zhou et al. also identified oxidation as a phenomenon that can hinder successful SLM processing and which must be avoided [9].

2 EXPERIMENTAL

Plasma-densified tungsten powder supplied by Tekna Advanced Materials (Macon, France) was subjected to selective laser melting under an argon atmosphere using a Renishaw AM125 system (Stone, UK). The system uses a high powered ytterbium fibre laser with a wavelength of 1070 nm, a maximum laser power of 200 W in continuous wave mode, a maximum laser scanning speed of 2000 mm/s and a laser beam diameter of 43 µm at the target surface. A commercially pure titanium substrate was used for the SLM experiments.

Figure 2 includes a scanning electron micrograph (SEM) showing the highly spherical powder morphology of the tungsten powder (insert). The analysis was carried out using a Jeol 6610 (Akishima, Japan) scanning electron microscope at 20kV. Also shown in Figure 2 is the powder particle distribution of the sub 45µm powder. The flow properties of the powder were also established through the 'conical' shape of the powder which were confirmed through measurements of the angle of repose (25.6°) which were carried out by LPW Technology (Runcorn, UK).

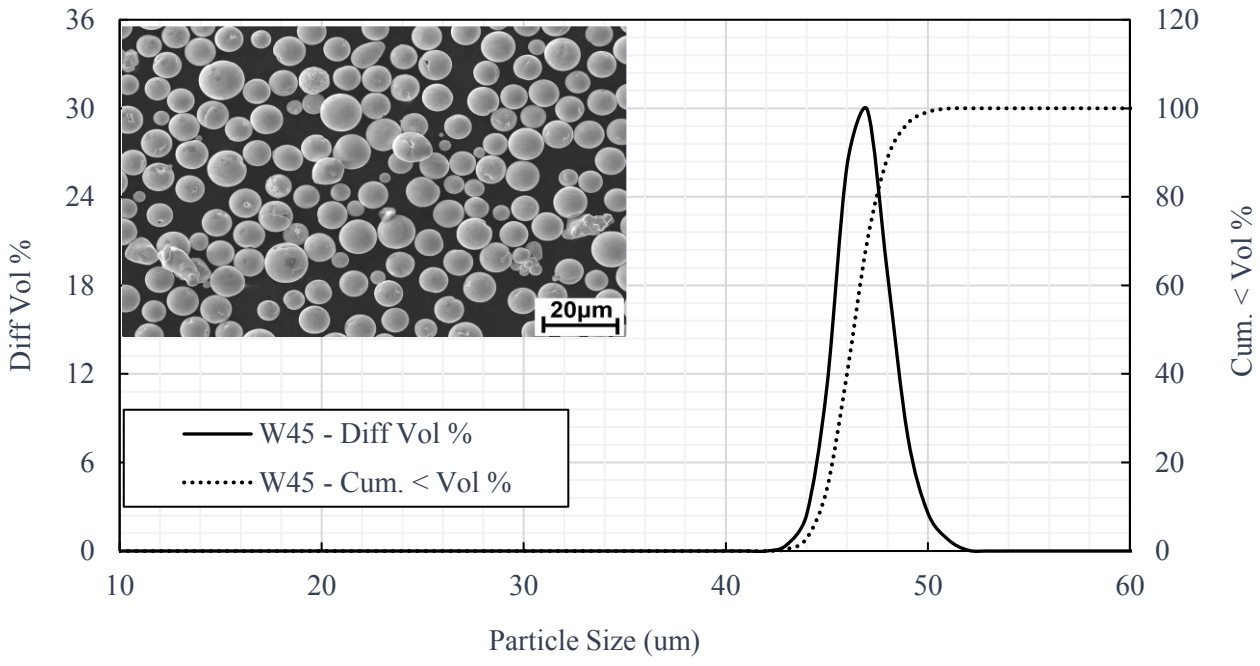

Figure 2: Powder morphology SEM (insert) and powder particle distribution for tungsten powder.

The selective laser melting of the tungsten powder was carried out by initially melting single layer melt tracks on the commercially pure titanium substrate. The purpose of this was to study the effect of

changing the scan speed on the formation of fusion lines and single tracks. The following step was to melt single layer hatch patterns with the aim of observing the effect of the scan strategy on the overlap hatch spacing. The final SLM step was fabricate tungsten block components (L=10mm, W=10mm and H=5mm) using a layer thickness of 30µm. The input laser energy was calculated and derived from 3D specific energy input and this was obtained by combining laser power, laser scan speed, powder layer thickness, and hatch spacing [15-18]. The 3D formulation can be seen as Equation 1 below:

$$\mathcal{E}_{Density} = \frac{P_{Laser}}{v_{scan} . S_{hatch} . t_{layer}} \quad \text{Eqn 1}$$

$\mathcal{E}_{\text{Density}}$ is the 3 dimensional input laser energy density, P_{laser} is the laser power, v_{scan} is the laser scan speed, s_{hatch} is the hatch spacing and t_{layer} is the layer thickness. The Renishaw AM125 machine uses a point exposure scan strategy which implies that the laser does not remain continuously on when incident on powder material. Therefore the scan speed was derived from the point distance and the exposure time used in the parameters.

The tungsten components that were fabricated using different processing parameters were then subjected to analysis alongside tungsten powder material on a Rigaku MiniFlex X-Ray diffraction (XRD) instrument (Tokyo, Japan). The tungsten block SLM specimens were also sectioned, ground, polished to 1µm in $Al_2 0_3$ powders and analysed for porosity levels using the light optical microscopy (LOM) and ImageJ image processing software. A selection of the polished specimens were then subjected to electrolytic etching and that was carried out using a 5% sodium hydroxide solution in a cooled electrolytic cell, at a typical temperature of -20°C at 40V. The etched samples were also analysed using LOM and SEM to study preferred growth direction of grains during the SLM process.

3 RESULTS

Tungsten powder was subjected to investigations which involved the creation of a process map through single track and single layer hatching studies. Figure 3 shows optical micrographs of the single track melting results of tungsten powder using different scan parameters. Figure 3 shows that when the energy density is insufficient ,i.e. as the laser speed increased due to increasing the point distance and decreasing the exposure time, the surface tension causes breaks which lead to thin melt tracks. With the increase of energy input which was achieved by lowering the point distance and increasing the exposure time, continuous melt tracks of increased width are formed. The increase of energy density is accompanied by an increase of the melt volume and a decrease of the melt viscosity, with melt hydrodynamics (driven by Marangoni effect) becoming more important [18]. Thus, decreasing the scanning speed causes the heat affected zone to become larger through melting of more tungsten powder.

Figure 4 shows the quantification of the melted line width for the tungsten as a function of the laser scanning speed. Figure 5 is a plot of the laser power as a function of the laser scan speed for the tungsten powder. It can be seen from Figure 4 and Figure 5 that the geometrical dimensions of the melt tracks are dependent on scan speed and on the energy density. This is useful information which can be used to define the threshold for the energy density. From Figure 4 and Figure 5, it is evident that for the given laser power the temperature and the volume of the molten powder is higher at lower scanning speeds and higher energy densities. Figure 4 shows the range of the line width against scanning speed for tungsten powder. The result also confirms that surface tension coefficient as well as melt viscosity decrease with increasing temperature [18] in the SLM of tungsten. Figure 5 shows the effect that varying the parameters has on the melt track volume and is a quantification of the processing window for the target line width for tungsten SLM.

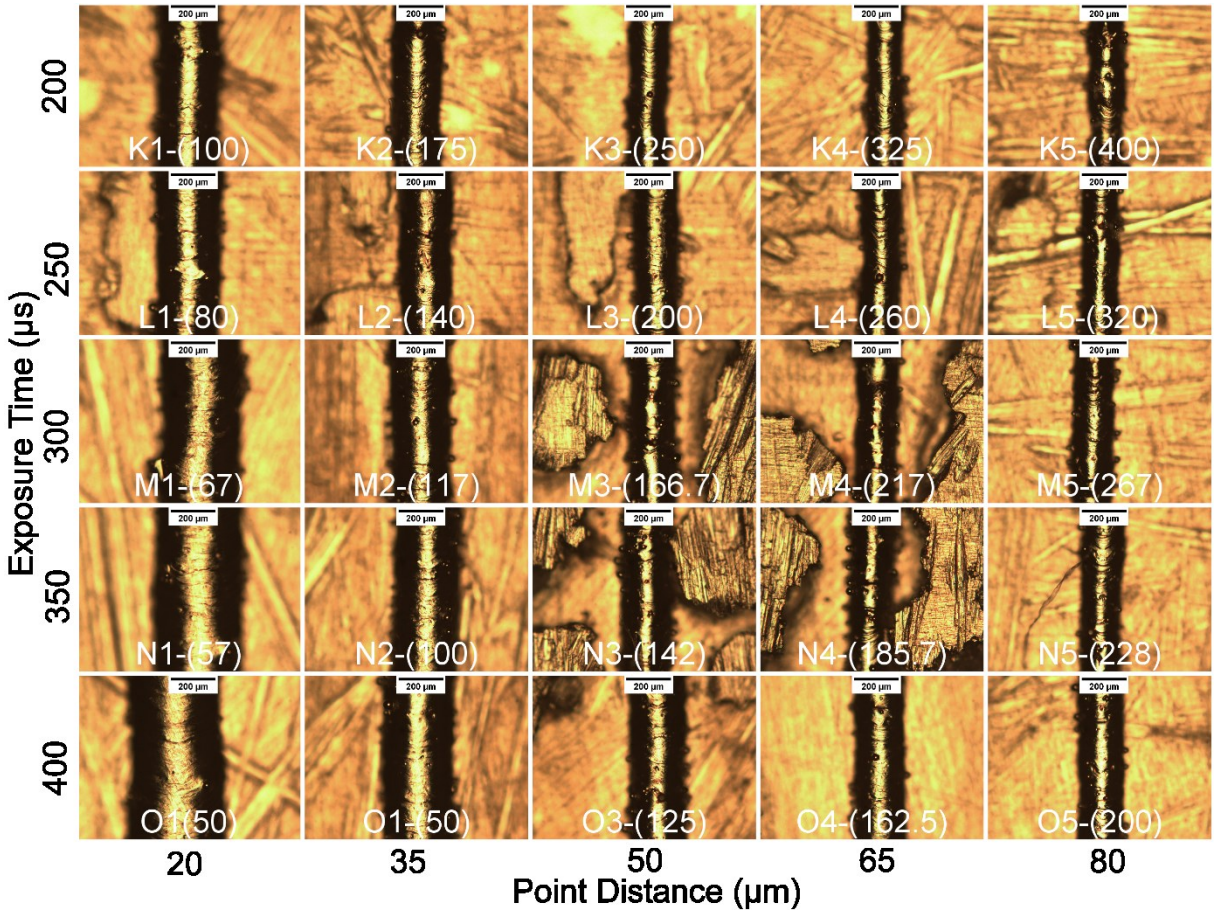

Figure 3: Single track melting results of tungsten powder using different scan parameters.

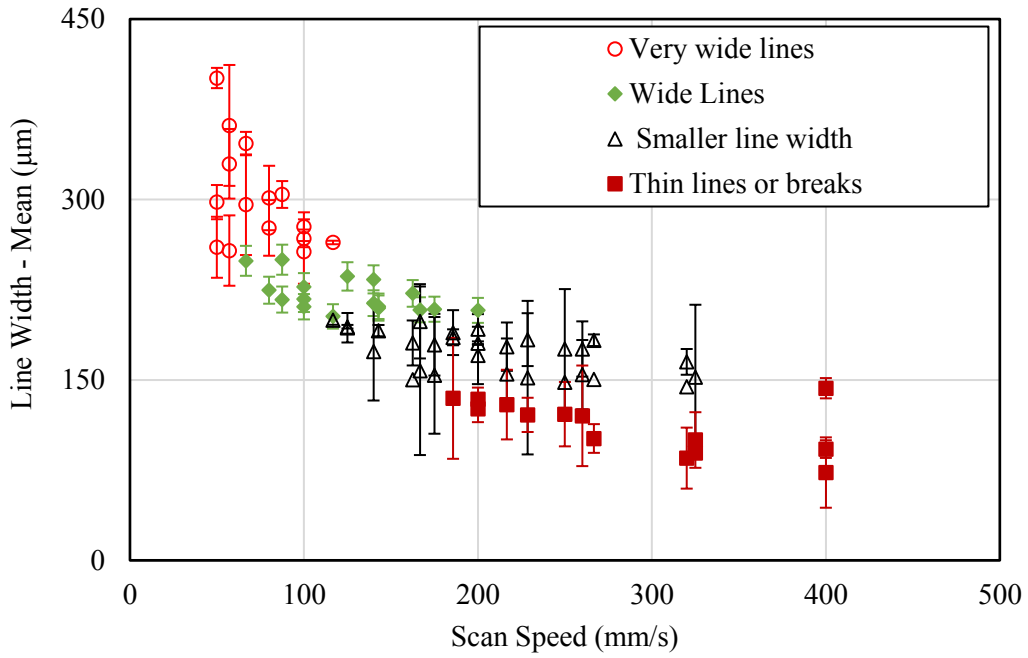

Figure 4: Line width vs scan speed for tungsten powder.

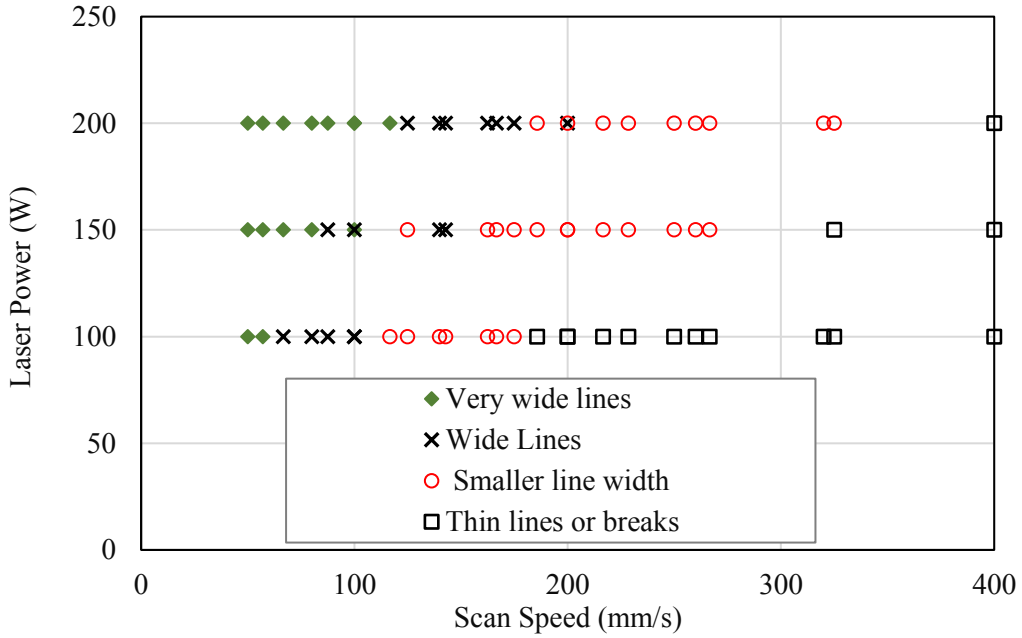

Figure 5: Laser power vs scan speed for tungsten powder.

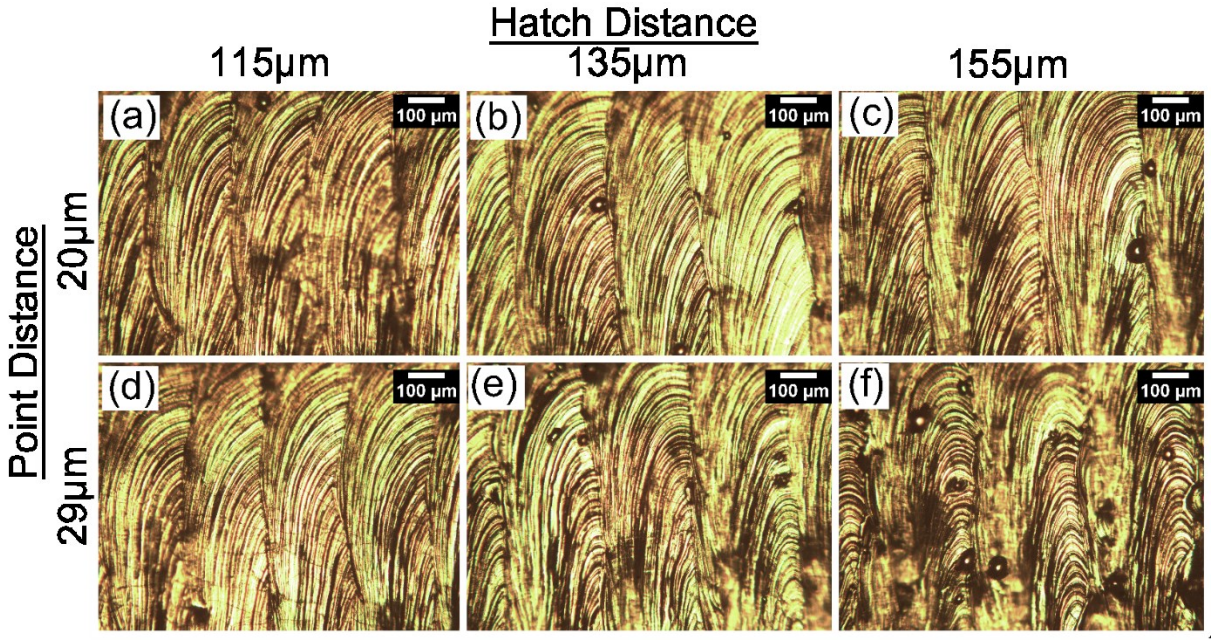

Figure 6: Single layer hatch patterns shown for tungsten using different processing parameters.

As it can be seen in the above studies, the laser power, scan speed or velocity can be modified with the result that the melt volume is either increased or reduced, but in the fabrication of 3 dimensional components, the hatch spacing and layer thickness have to be taken into consideration as shown in Eqn 1. In conjunction with the laser power, scanning speed, the hatch spacing and layer thickness can be modified to increase or decrease the 3D laser energy density in order to control the powder fusion. These process parameters have been used in this study with powder material properties of tungsten having been taken into consideration and the threshold determined by the previously outlined studies [19]. Figure 6 shows the single layer hatch patterns for tungsten using different processing parameters at the laser power of 200W and exposure time of 200µs. Also shown in Figure 6 are the hatch distance and point distance processing parameters. The result shows that at a given laser power, higher point

distance and hatch spacing reduce the size of the melt pool spreading and affect the overlap [20]. The results show the effect of the high thermal conductivity of tungsten in that a relatively high overlap is required (~50%) in comparison to other materials such as stainless steel. The results also indicate that insufficient overlap of the scan tracks could result in fusion defects or porosity [20].

Using the laser power of 200W and exposure time of 200µs, tungsten blocks were fabricated using a layer thickness of 30µm. The point distance and the hatch distance were varied as shown in Figure 7. The samples (width=10mm, length=10mm and height=5mm) were successfully fabricated without any visible defects or delamination during the melting process and a relatively smooth surface was produced. Figure 7 shows the SEM's of the top surfaces of SLM tungsten fabricated. However, at higher magnification surface cracks are visible within the manufactured components. It can be seen from Figure 7 that the volume of unmelted adherent particles was reduced when the tungsten was melted using a point distance of 20µm and a hatch spacing of 115µm (Figure 7 (a)).

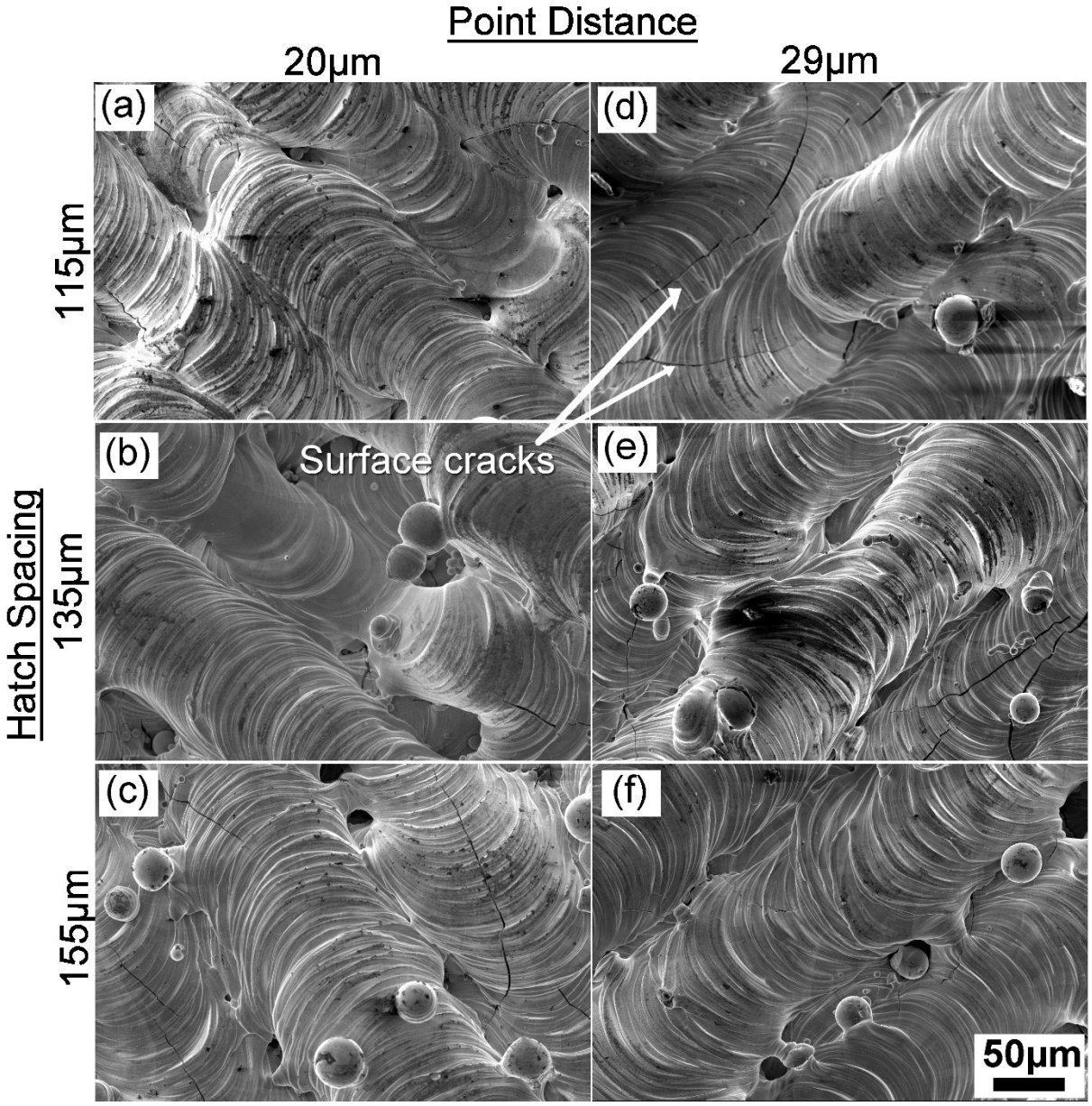

Figure 7: SEM's of the top surfaces of SLM tungsten manufactured using different parameters.

Figure 8 shows the results of the phase identification using an X-ray diffraction of the cross sectional view (XY) and build direction view (ZY) of SLM samples fabricated using a laser power of 200W, hatch spacing of 115µm, point distance of 20 µm, exposure time of 200µs and layer thickness of 30µm.

Compared to W powder, the diffraction peaks of the selective laser melted samples of W exhibit stronger intensity along direction (100) and (211). Thus, it can be deduced that the growth from the melt pool formed from the melted metal powder favoured solidification in the orientation along a preferred direction along which grain refinement process took place [21]. Furthermore minor peaks were observed in the build-direction (c) of the SLM tungsten along the 110 and the 211 direction, suggesting a strong preferential growth along the build direction.

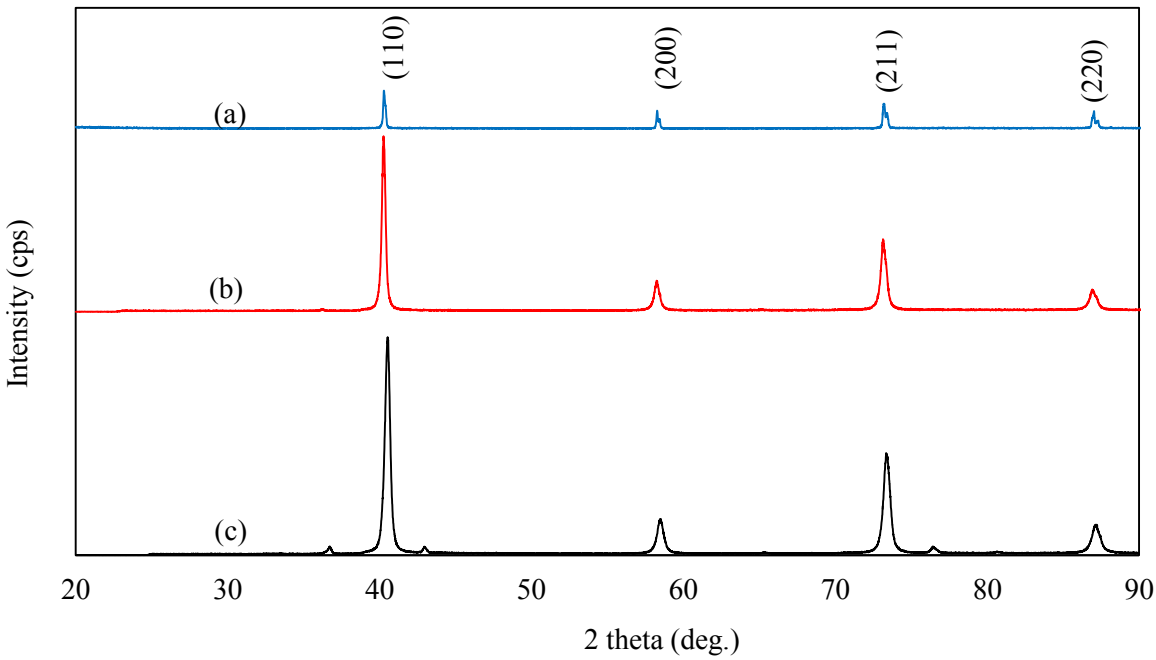

Figure 8: X-ray diffraction plot showing the phase identification using an X-ray diffraction of the powder (a), cross sectional view (b) and build direction view (c) of SLM samples.

Figure 9 shows the results of the tungsten density as a function of the 3D volume energy density. The density values shown in Figure 9 were optically determined, in the cross-sectional view (xy) of the tungsten samples. It can be seen from Figure 9 that specimens manufactured using the increased energy density of 580 J/mm^3 had the highest density and increasing the energy density any further did not lead to improvement in the density. Figure 9 shows the effect of the different processing parameters for the SLM of tungsten part integrity.

Optical micrographs showing cross sectional (xy) and build direction (zy) grain structures are shown in Figure 10 (a and b). The results show the grain structures for the parts that had a high density and were fabricated using a 3D laser energy density of 580 J/mm^3. The cross-sectional (xy) grains are distinct form the build directional (zy) grain structures. The optical micrographs confirm that there is a strong preferential growth and prevalent anisotropy is tungsten manufactured using the SLM process. The higher magnification of the grain alignment and crack initiation zones are shown in scanning electron micrographs in Figure 10 (c and d) for both cross sectional (xy) and build direction (zy) views. Figure 10 (a) shows that there is an organisation of grain texture in accordance with scan tracks. Figure 10 (b) shows that when the build direction (zy) texture is analysed, there is anisotropy as grains align along the build direction as expected because SLM is a layer by layer deposition, melting and freezing process.

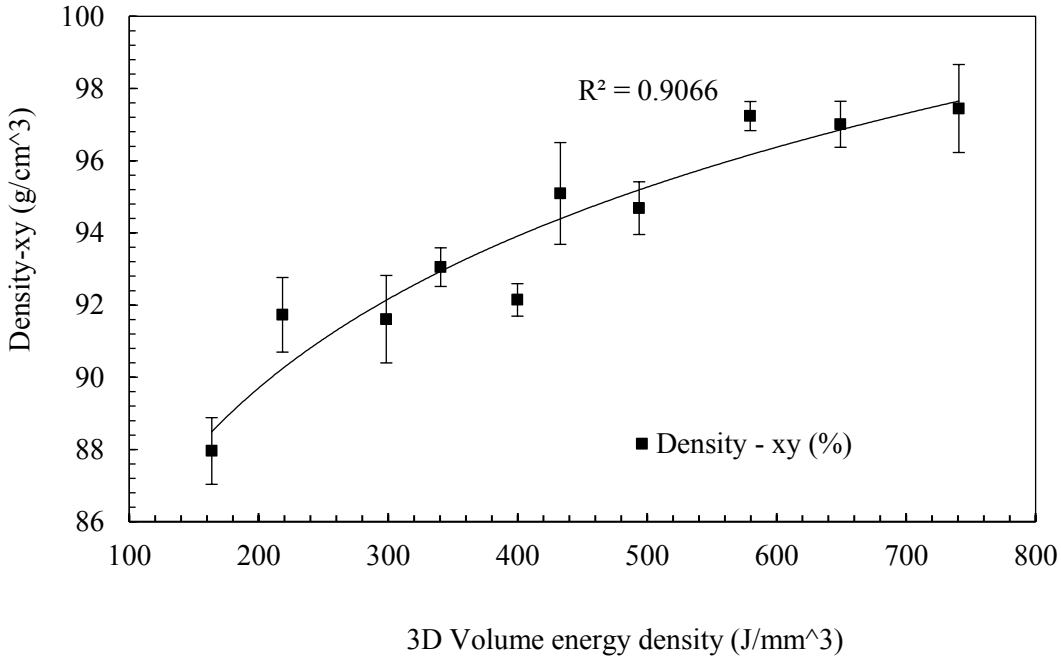

Figure 9: Optically determined density of the lateral view as a function of 3D volume energy density.

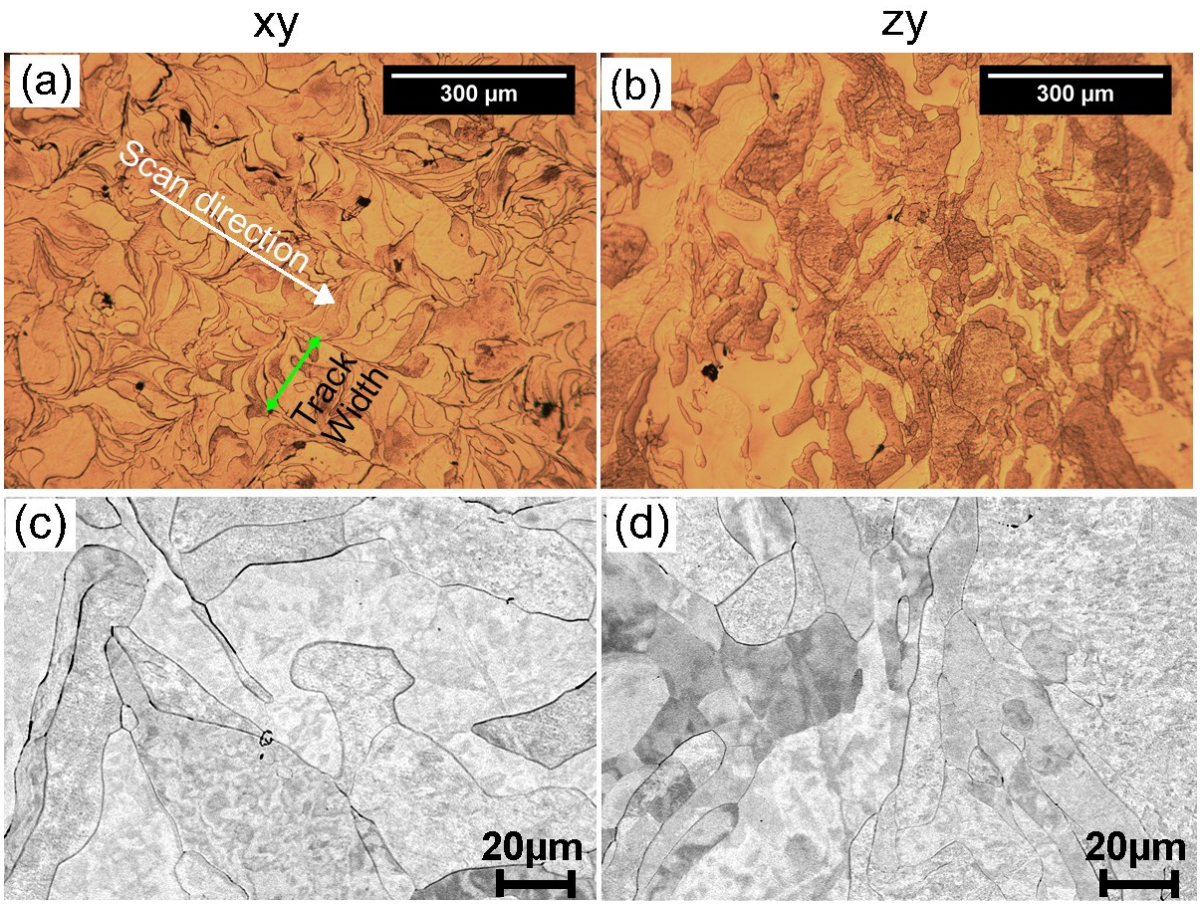

Figure 10: Optical micrographs showing cross sectional (a) and build direction (b) grain structures. High magnification SEMs showing crack initiation zones showing cross-sectional (c) and build directional (d).

4 DISCUSSION

Refractory metals such as pure tungsten are considered difficult to manufacture using SLM due to the high melting point, high thermal conductivity, high viscosity and oxidation sensitivity. In this study we have investigated processing parameters with the aim of overcoming the high cohesive energy, high surface tension and of reducing the balling phenomenon, all of which have been reported to hinder the successful processing of pure tungsten using SLM. This study helped analyse the mode of melting for the tungsten powder. The processing started with the single melt pool strategy where it was demonstrated that there is a dependence of single tracks dimensions on the energy density and this was decisive in the selection of the range of the energy density to use. It has been shown that the parameters for melting tungsten depend on the energy density and scan speed, and that point distance has a significant role overall. The high energy density level that were resultant from slow scanning speed have led to high density parts, and have thus been found to be compatible with the high thermal conductivity of the tungsten which leads it to cool very rapidly. The processing has also been carried out in an argon atmosphere to prevent oxidation which has been reported to lead to the formation of an oxide film on the surface of previously built solid tracks and at the bottom of the melt pools [9].

5 CONCLUSION

In this study, the interaction of pure tungsten powder with processing conditions in selective laser melting has been considered. The role of the pure tungsten powder interaction with processing conditions within SLM has been demonstrated using different parameters which are equivalent to different energy densities. The process quality was quantified in terms of porosity and density where densities of up to 98% were achieved. The analysis of the microstructure has shown the anisotropy present in solids produced during the SLM processing of tungsten.

6 REFERENCES

[1] A.T. Sidambe, "Biocompatibility of Advanced Manufactured Titanium Implants-A Review", *Materials*, 2014, vol. 7, no. 12, pp. 8168-8188.
[2] M.T. Andani, N. Shayesteh Moghaddam, C. Haberland, D. Dean, M.J. Miller, M. Elahinia, "Metals for bone implants. Part 1. Powder metallurgy and implant rendering", *Acta Biomaterialia*, 2014, vol. 10, no. 10, pp. 4058-4070.
[3] P. Fox, S. Pogson, C.J. Sutcliffe, E. Jones, "Interface interactions between porous titanium/tantalum coatings, Selective Laser Melting (SLM), on a cobalt–chromium alloy", *Surface & Coatings Technology*, 2008, vol. 202, no. pp. 5001–5007.
[4] A.T. Sidambe, I. Todd, P.V. Hatton, "Effects of build orientation induced surface modifications on the in vitro biocompatibility of electron beam melted Ti6Al4V", *Powder Metallurgy*, 2016, vol. 59, no. 1, pp. 57-65.
[5] O. Ivanova, C. Williams, T. Campbell, "Additive manufacturing (AM) and nanotechnology: promises and challenges", *Rapid Prototyping Journal*, 2013, vol. 19, no. 5, pp. 353-364.
[6] R. van Noort, "The future of dental devices is digital", *Dent. Mater.*, 2012, vol. 28, no. 1, pp. 3-12.
[7] N.J. Harrison, I. Todd, K. Mumtaz, "Reduction of micro-cracking in nickel superalloys processed by Selective Laser Melting: A fundamental alloy design approach", *Acta Mater.*, 2015, vol. 94, no. pp. 59-68.
[8] P. Vora, K. Mumtaz, I. Todd, N. Hopkinson, "AlSi12 in-situ alloy formation and residual stress reduction using anchorless selective laser melting", *Additive Manufacturing*, 2015, vol. 7, no. pp. 12-19.
[9] X. Zhou, X.H. Liu, D.D. Zhang, Z.J. Shen, W. Liu, "Balling phenomena in selective laser melted tungsten", *J Mater Process Tech*, 2015, vol. 222, no. pp. 33-42.

[10] R. Wauthle, J. van der Stok, S. Amin Yavari, J. Van Humbeeck, J.P. Kruth, A.A. Zadpoor, H. Weinans, M. Mulier, J. Schrooten, "Additively manufactured porous tantalum implants", *Acta Biomater*, 2015, vol. 14, no. pp. 217-225.
[11] R. Li, M. Qin, C. Liu, H. Huang, H. Lu, P. Chen, X. Qu, "Injection molding of tungsten powder treated by jet mill with high powder loading: A solution for fabrication of dense tungsten component at relative low temperature", *International Journal of Refractory Metals and Hard Materials*, 2017, vol. 62, Part A, no. pp. 42-46.
[12] K. Deprez, S. Vandenberghe, K. Van Audenhaege, J. Van Vaerenbergh, R. Van Holen, "Rapid additive manufacturing of MR compatible multipinhole collimators with selective laser melting of tungsten powder", *Med. Phys.*, 2013, vol. 40, no. 1, pp. 012501.
[13] M. Zhong, W. Liu, G. Ning, L. Yang, Y. Chen, "Laser direct manufacturing of tungsten nickel collimation component", *J Mater Process Tech*, 2004, vol. 147, no. 2, pp. 167-173.
[14] R. Ebert, F. Ullmann, D. Hildebrandt, J. Schille, L. Hartwig, S. Kloetzer, A. Streek, H. Exner, "Laser Processing of Tungsten Powder with Femtosecond Laser Radiation", *J Laser Micro Nanoen*, 2012, vol. 7, no. 1, pp. 38-43.
[15] B. Brown, "Characterization of 304L stainless steel by means of minimum input energy on the selective laser melting platform", 2014, Master Of Science Manufacturing Engineering, Missouri University Of Science And Technology.
[16] D. Gu, Y. Shen, "Balling phenomena in direct laser sintering of stainless steel powder: Metallurgical mechanisms and control methods", *Materials & Design*, 2009, vol. 30, no. 8, pp. 2903-2910.
[17] Y.Q. Yang, J.B. Lu, Z.Y. Luo, D. Wang, "Accuracy and density optimization in directly fabricating customized orthodontic production by selective laser melting", *Rapid Prototyping Journal*, 2012, vol. 18, no. 6, pp. 482-489.
[18] I. Yadroitsev, P. Bertrand, I. Smurov, "Parametric analysis of the selective laser melting process", *Appl Surf Sci*, 2007, vol. 253, no. 19, pp. 8064-8069.
[19] L.E. Criales, Y.M. Arısoy, B. Lane, S. Moylan, A. Donmez, T. Özel, "Predictive modeling and optimization of multi-track processing for laser powder bed fusion of nickel alloy 625", *Additive Manufacturing*, 2017, vol. 13, no. pp. 14-36.
[20] J.J.S. Dilip, G.D.J. Ram, T.L. Starr, B. Stucker, "Selective laser melting of HY100 steel: Process parameters, microstructure and mechanical properties", *Additive Manufacturing*, 2017, vol. 13, no. pp. 49-60.
[21] D. Zhang, Q. Cai, J. Liu, "Formation of Nanocrystalline Tungsten by Selective Laser Melting of Tungsten Powder", *Materials and Manufacturing Processes*, 2012, vol. 27, no. 12, pp. 1267-1270.